Mon. Not. R. Astron. Soc. **356,** 1357–1361 (2005) doi:10.1111/j.1365-2966.2004.08564.x

New giant H II regions in the southern sky

V. Firpo,[1]★ G. Bosch[1]† and N. Morrell[2]†‡

[1]*Facultad de Ciencias Astronómicas y Geofísicas, Universidad Nacional de la La Plata, Paseo del Bosque s/n, 1900 La Plata, Argentina*
[2]*Las Campanas Observatory, Carnegie Observatories, Casilla 601, La Serena, Chile*

Accepted 2004 October 27. Received 2004 October 26; in original form 2004 April 27

ABSTRACT

We present results of a search for giant H II regions in southern galaxies. Using high-resolution spectra, obtained with the Magellan Inamori Kyocera Echelle (MIKE) at the Las Campanas Magellan II telescope, we were able to resolve the emission-line profiles and determine the intrinsic velocity dispersion of the ionized gas. Out of four observed regions, selected from previous CCD narrow-band photometry, we detected three H II regions showing supersonic velocity dispersion, characteristic of giant H II regions, and their location in diagnostic diagrams suggests that a powerful starburst is the source of ionization energy.

Key words: H II regions – galaxies: individual: NGC 2997 – galaxies: individual: NGC 7552 – galaxies: starburst.

1 INTRODUCTION

Giant extragalactic H II regions (GHIIRs) are extended, luminous objects, which are observed in the discs of spirals and in irregular galaxies. GHIIRs are formed as a result of the presence of a large number of young and massive stars, the ultraviolet flux of which ionizes the surrounding gas. Smith & Weedman (1970) found that the emission-line profile widths of the giant H II regions correspond to supersonic velocities in the gas. This behaviour is still not clearly explained, but it allows us to distinguish giant H II regions from an agglomeration of classic H II regions by means of high-resolution spectroscopy.

Analysing information for different galaxies, Melnick (1979) found a narrow correlation between the total luminosity of GHIIRs and the supersonic widths of emission-line profiles. Independent investigations confirmed the existence of such a regression but found different values for its slope (Terlevich & Melnick 1981; Roy, Arsenault & Joncas 1986; Hippelein 1986), which has generated parallel theories to explain this phenomenon, invoking dynamics of virialized systems (Tenorio-Tagle, Muñoz-Tuñón & Cox 1993), superposition of multiple gas bubbles in expansion (Chu & Kennicutt 1994), or turbulence of the same interstellar gas (Medina Tanco et al. 1997). Although the supersonic widths obtained by different authors agree within the expected errors, there are remarkable differences in the determined fluxes and therefore in the corresponding luminosities. Bosch, Terlevich & Terlevich (2002) obtained narrow-band CCD photometry of emission lines from a group of GHIIRs, including a detailed analysis of their evolutionary state. Discarding those regions that show signs of evolution, Bosch et al. (2002) found a very narrow regression in the plane luminosity (L) versus velocity dispersion (σ). However, the remaining sample was noticeably reduced and thus the number of objects suitable for the correlation needs to be increased so that the regression has statistical significance. Therefore new GHIIRs must be found.

Inspecting the list of known GHIIRs used in these studies, it is evident that all of them belong to the northern hemisphere, with the exception 30 Doradus in the Large Magellanic Cloud. Making use of narrow-band CCD photometry, Feinstein (1997) has found some very luminous H II regions when analysing the brightness distribution of such regions in spiral galaxies of the southern sky, several of them with luminosities that differ from those expected from the H II region luminosity function estimated for each galaxy. These are our candidates for giant H II regions in the southern sky. To verify the giant nature of these H II regions, we need high-resolution spectra to measure the emission-line profile widths and to estimate if the velocity dispersion is really supersonic.

In this paper we present echelle data obtained at Las Campanas Observatory (LCO) of four GHIIR candidates in the galaxies NGC 7552 and 2997. The goal of this work was to determine the velocity dispersion which broadens the profile of the emission lines. The high signal-to-noise ratio, together with the high resolution of the echelle data, allowed us to resolve the profile of the emission lines and to calculate the velocity dispersion of the ionized gas. This analysis was performed by measuring the true width of the emission line profile after correcting the observed one by the instrumental profile and thermal contribution. The observations are described in Section 2, the data reduction steps are outlined in Section 3, and the results obtained are presented in Section 4.

2 OBSERVATIONS

High-dispersion spectra were obtained by one of the authors (NM) at the 6.5-m Magellan II (Clay) Telescope, LCO, on 2002

★E-mail: vero@carina.fcaglp.unlp.edu.ar
†Member of Carrera del Investigador Científico, CONICET, Argentina.
‡On leave from Facultad de Ciencias Astronómicas y Geofísicas, Universidad Nacional de La Plata.

Table 1. Log of observations for the GHIIR candidates and flux standard stars.

Date	NGC	Exp.	Airmass	Standard	Airmass
2002 Dec 20	7552 I	1800	1.28	HR 1544	1.87
	2997 II	1030	1.00	HR 4468	1.15
2002 Dec 21	2997 I	1800	1.07	HR 4468	1.17
	2997 II	2400	1.19	HR 4468	1.17
	7552 IV	2400	1.29	HR 1544	1.83

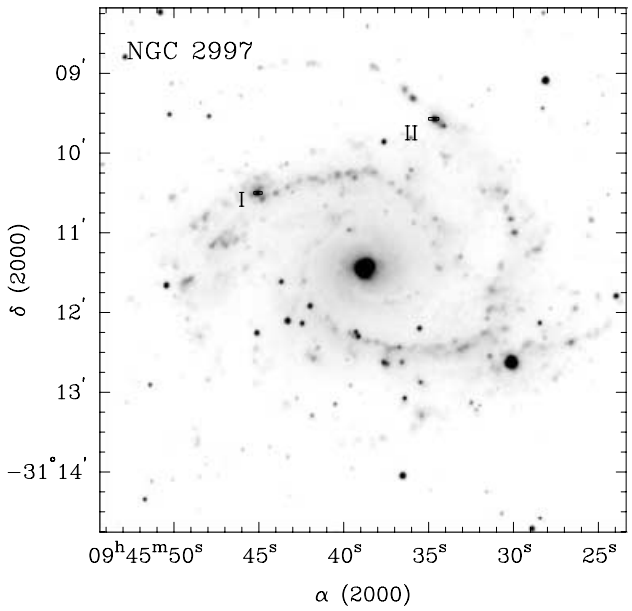

Figure 1. Finding chart for GHIIR candidates observed in NGC 2997, identified by rectangles that resemble slit position and orientation. The Hα images were kindly made available by C. Feinstein.

December 20–21. The observations were obtained using the echelle double spectrograph Magellan Inamori Kyocera Echelle (MIKE). The spectral range covered by the observations was from 3500 to 4600 Å for the blue side, and from 4500 to 7300 Å for the red one. The effective slit width was 1 arcsec. The spectral resolution for this instrument configuration is $\Delta\lambda = 0.117$ Å pixel^{-1} at 5400 Å, equivalent to 7 km s^{-1} pixel^{-1}. The precision in the determination of the centroid of a spectral line is therefore about 0.012 Å or its equivalent in radial velocity of less than 1 km s^{-1}. The data were binned by 3 pixels in the spatial direction, to minimize readout contribution to final spectrum noise.

Table 1 lists the observed regions and standard stars, together with their airmasses and exposure times. The exposure time for standard stars was 5 s. Figs 1 and 2 show the finding charts for the observed H II regions.

In addition, Th–Ar comparison spectra, quartz lamp flat-fields and bias frames were taken every night.

3 DATA REDUCTION

The data analysis was carried out using IRAF[1] software. The bidimensional images were bias-corrected as usual, but we decided not to apply flat-field corrections because we found that the quartz lamp did not fairly reproduce the illumination conditions of the weak sources analysed here.

[1] Image Reduction and Analysis Facility.

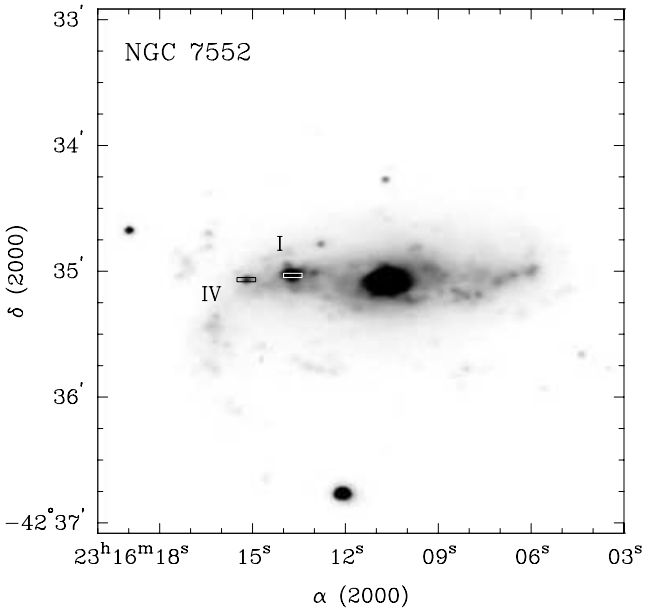

Figure 2. As Fig. 1, for NGC 7552.

H II regions show a weak continuum, so it is not possible to register a good signal in the bidimensional image in order to trace the spectrum along the detector. In order to extract the spectra, it was therefore necessary to use a standard star spectrum as an aperture template. The star apertures were then copied over the spectrum of the corresponding H II region after modifying only the aperture size and centre to account for the extended nature of our science targets.

We performed flux calibrations using the observed spectrophotometric standard stars. However, the fluxes presented here should be regarded as only a first-order approximation. As mentioned before, we could not perform a reliable flat-field correction, and this turned out to be important as the strongly varying sensitivity over the echelle orders was difficult to take into account. Moreover, the observed standard stars have their fluxes tabulated every 16 Å, and the number of defined intervals within an echelle order ranged from 4 to 10, depending on the quality of the spectrum. Finally, because of their extended nature, part of the observed H II regions lay outside the spectrograph slit, and consequently absolute fluxes cannot be obtained from our data.

Fig. 3 shows Hα and [N II] lines in our calibrated spectra, including the Gaussian profiles fitted to the emission lines and used to derive central wavelengths and velocity dispersions.

4 RESULTS

4.1 Line intensities

We identified the Hα line $\lambda_{\rm lab} = 6562.817$ Å together with the [N II]6548- and 6584-Å lines. For each H II region we calculated the target redshift by fitting a Gaussian profile to the Hα line, and used this redshift to identify the other spectral lines. Fluxes were measured for lines in the central 400 Å of each order, avoiding the order edges because of their low signal. Flux measurements for different emission lines in the spectra of the observed H II regions are

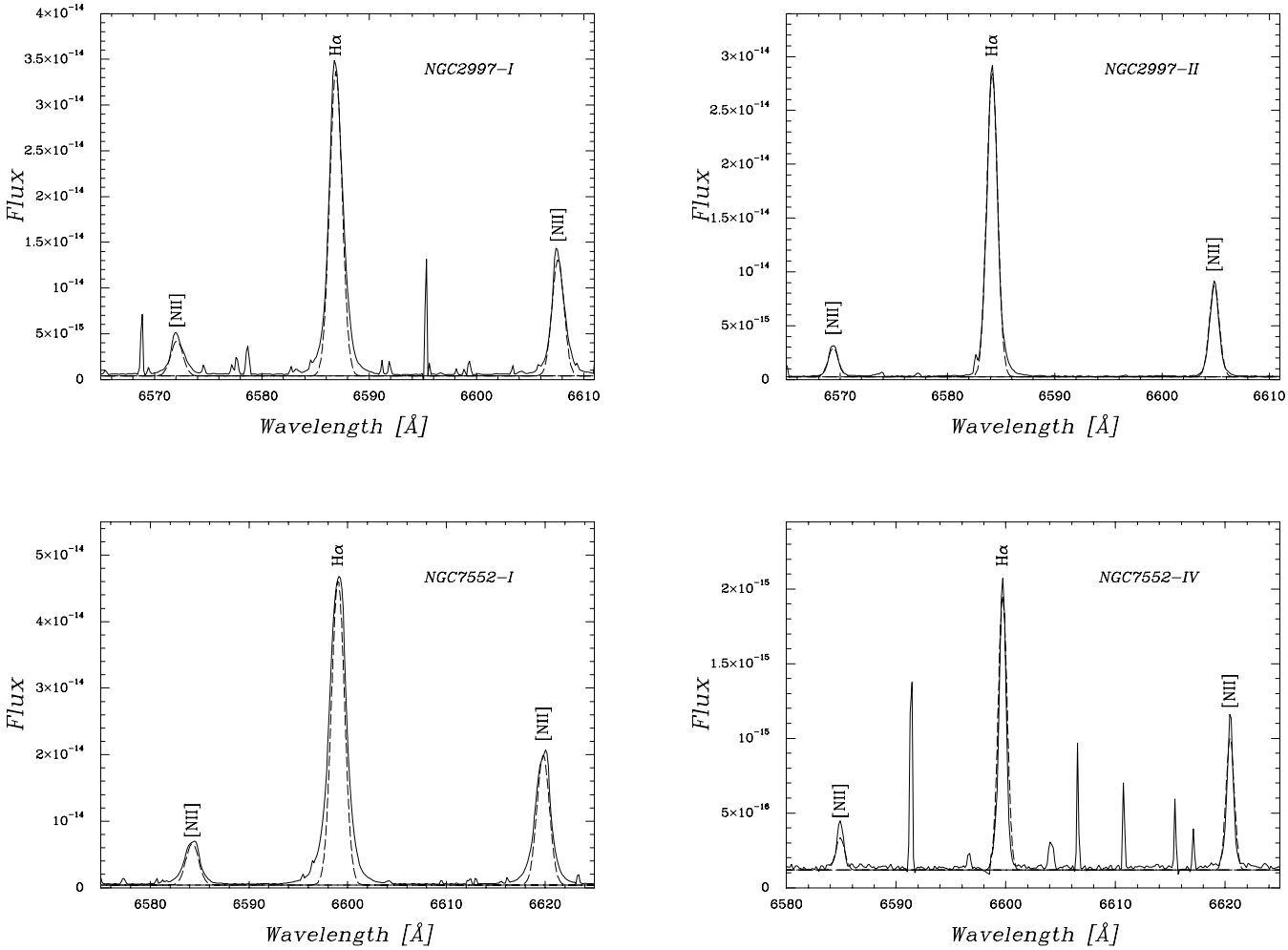

Figure 3. Flux- and wavelength-calibrated spectra from our GHIIR candidates. These illustrate the high signal-to-noise ratio obtained for the target regions and the varying relative intensities between Hα and the [N II] lines.

presented in Table 2 in units of the Hβ flux. Flux ratios to Hβ were corrected for extinction using the standard extinction curve.

These relative fluxes should be considered as reference only, as the lack of proper flat-fielding described in the previous section prevented us from obtaining a reliable flux calibration. The same caveat applies for our reddening correction, as it was derived from the Hα/Hβ line ratio, which involves two spectral features that lie well apart on the two-dimensional image. We did, however, estimate line ratios for ions present in the same echelle order, such as [O III]λ5007/Hβ, [S II]λ6725/Hα or [N II]λ6584/Hα which are further discussed in Section 5.

4.2 Heliocentric radial velocities

The individual radial velocity of each spectral line listed in Table 3 was obtained by measuring the central wavelength determined from the Gaussian profile fitting.

The measured radial velocities for the two regions of NGC 2997 present well-known differences. Milliard & Marcelin (1981) built a catalogue of 382 H II regions, giving their Hα fluxes, diameters, positions and radial velocities for some of them. They derived an inclination of about 40° for the galactic plane relative to the plane of the sky, and a systemic velocity of 1090 km s^{-1}. Sperandio et al. (1994) found a similar result using an independent data set.

Table 2. Emission lines identified in our spectra. Intensity ratios relative to Hβ are corrected for extinction, although they should be used mainly as a reference value (see text). Lines marked with an asterisk are those that contribute to the determination of the average value of the turbulent velocity.

λ(Å)	Ion	2997 I	2997 II	7552 I	7552 IV
3726	[O II]	1.26*	3.28*	2.33*	...
3729	[O II]	1.55*	4.02*	2.72*	...
3888	H8+He I	...	0.83	...	...
3970	Hϵ	...	0.74	0.31*	...
4102	Hδ	0.53	0.50*	0.64	...
4340	Hγ	0.66	1.05*	0.76*	...
4861	Hβ	1.00*	1.00*	1.00*	1.00*
4959	[O III]	0.13	0.29*	...	...
5007	[O III]	0.43*	0.92*	0.30*	...
5876	He I	0.08	...	0.08	...
6300	[O I]	0.03*	...	0.02	...
6548	[N II]	0.33*	0.26*	0.36*	0.51*
6563	Hα	2.84*	2.84*	2.84*	2.84*
6584	[N II]	1.03*	0.74*	1.12*	1.29
6679	He I	...	...	0.02	...
6717	[S II]	0.33*	0.15*	0.26*	0.36*
6731	[S II]	0.25*	0.11*	0.21*	0.57*
7065	He I	...	...	0.01	...
7136	[Ar III]	0.03*	0.05*	0.05*	...

Table 3. Kinematical data derived for the observed H II regions. Heliocentric radial velocities are listed in column 2, and the average value of the turbulent velocity σ is shown in column 3. Column 4 gives an indication of the uncertainty in the estimation of the turbulent velocity, obtained after averaging over a number n of emission lines, shown in column 5. All radial velocities are listed in km s^{-1}.

NGC	Rad. Vel.	Vel. Disp.	Error	n
2997 I	1113	25	2	11
2997 II	919	21	2	13
7552 I	1619	36	1	12
7552 IV	1647	9	3	5

The average value of our radial velocities for regions NGC 2997 I and NGC 2997 II agrees with the published data and the difference between them is explained by galactic rotation. It is also worth noting that the radial velocity for NGC 2997 published in the Sandage & Bedke (1988) atlas is 799 km s^{-1}. This value was adopted by Feinstein (1997), and we will consider this issue again when we estimate the distance to the NGC 2997 galaxy.

The radial velocity obtained in the present work of the two regions observed in the NGC 7552 galaxy does not differ from the previously published data (de Vaucouleurs et al. 1991).

4.3 Velocity dispersion

The physical parameter that we wish to measure is the turbulent velocity of the ionized gas (σ). Nevertheless, the observed profile (σ_o) includes the contribution of thermal random motion (σ_t) and the instrumental profile (σ_i) introduced by the spectrograph. Therefore we can obtain the true velocity dispersion $\sigma^2 = \sigma_o^2 - \sigma_i^2 - \sigma_t^2$.

Assuming that the observed regions have a typical kinetic temperature $T = 10^4$ K, we estimated the thermal component of the linewidth for the observed regions. The instrumental profile width was determined from narrow emission lines present in the Th–Ar lamp and found to be approximately 7 km s^{-1}. The errors in the determination of the turbulent velocity have been calculated using the observational errors in σ_o and assuming uncertainties of ± 2000 K in the temperature and negligible errors in σ_i. Table 3 shows the average value of the turbulent velocity for each region. The average value was derived using lines with profiles that are well defined and have a high signal-to-noise ratio, and all of them have been corrected by its corresponding thermal broadening. Emission lines that match these requirements are flagged with an asterisk in Table 2. We have discarded the lines with velocity dispersions that were deviant from the average by 2σ or more. For the adopted $T = 10^4$ K kinetic temperature, the sound speed is about 13 km s^{-1}. Three out of the four observed H II regions present velocity dispersions higher than that value, as seen in Table 3, then confirming their identification as GHIIRs. However, for NGC 7552 IV we have estimated a velocity dispersion of 9 km s^{-1}, suggesting that this one is most probably a classic H II region.

5 ANALYSIS

5.1 Mechanism of excitation

In order to estimate the electronic temperature in our H II regions, we need to measure the intensity ratio for pairs of emission lines emitted by a single ion from two levels with different excitation energies. However, due to our large wavelength resolution, we could not measure reliable intensities for the weaker emission lines.

Rola, Terlevich & Terlevich (1997) analysed the use of diagnostic diagrams to derive the mechanism of excitation present in H II galaxies. Although we are dealing with less energetic regions, we can still use these diagrams to identify the source of excitation for our observed recombination lines. We could build two diagrams (from a set of four proposed by Rola et al. 1997):

(1) [O III]λ5007/Hβ versus [S II]λ6725/Hα;
(2) [O III]λ5007/Hβ versus [N II]λ6584/Hα.

Rola et al. (1997) used photoionization models of OB stars to determine the limit between H II galaxies and other type of active galaxies in the diagnostic diagrams. Fig. 4 represents these diagrams, including the curves obtained by these authors from models considering effective stellar temperatures of 50 000 K (dashed line) and 60 000 K (full line), respectively. Two regions are defined in these diagrams: a lower left region, for objects whose mechanism of excitation must be photoionization by OB stars; and an upper right region, for objects whose ionizing energy source must come from jets or shocks (such as in Seyfert 2s and LINERs). Our GHIIRs lie on the former region of the diagram, hence we can confirm that their mechanism of excitation is photoionization by stars. We can therefore rule out the possibility that the observed excitation in the NGC 7552 I region is produced by UV photons originating in the galaxy nucleus (Durret 1990). It is worth noting that large values derived for the [N II]λ6584/Hα ratio suggest that we are probably

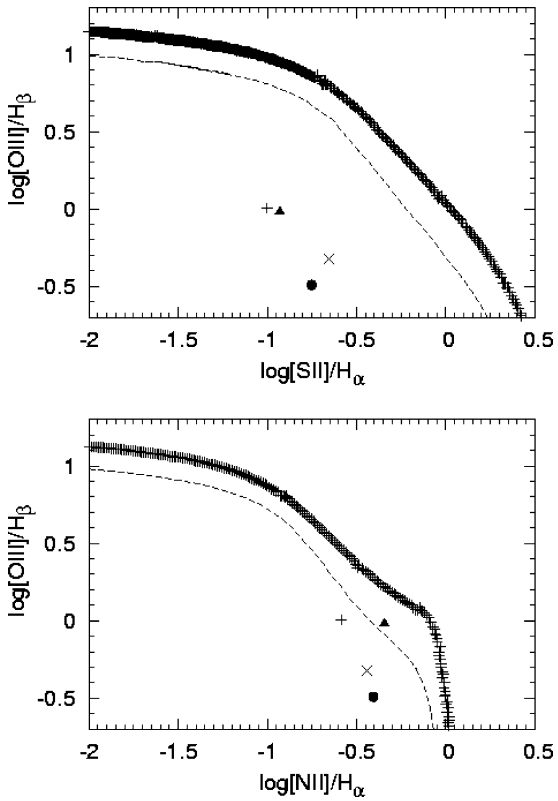

Figure 4. Two diagnostic diagrams used in the characterization of the observed regions. The curves correspond to models of photoionization by OB stars, for stellar effective temperatures of 50 000 K (dashed line) and 60 000 K (full line) (Rola et al. 1997). NGC 2997 I is represented by a cross; NGC 2997 II by a plus sign; NGC 7552 I by a circle and NGC 7552 IV by a triangle.

dealing with high-metallicity regions. However, a complete analysis of proper abundance indicators, such as N/O (Garnett 1990), are needed to confirm this.

5.2 Luminosities

Having discovered the giant nature of three out of the four candidate regions, we can check their location in the log L versus log σ diagram. In order to do this we must review their luminosities.

We corrected the Hα luminosities obtained by Feinstein (1997) for the contamination due to [N II]. Feinstein (1997) disregarded this correction as he was looking for the luminosity function within each galaxy. We could correct each luminosity individually, however, because our spectra provided the necessary spectroscopic information. We found that the values of the correction Hα/(Hα + [N II]) were different for each one of the regions. These values varied from 0.61 (NGC 7552 IV) to 0.74 (NGC 2997 II).

As mentioned in Section 4.2, it was necessary to re-calculate the distance to NGC 2997, using the radial velocity estimated by Milliard & Marcelin (1981) and a Hubble constant of 75 km s^{-1} Mpc^{-1}. The value of the distance found for the NGC 2997 galaxy was 17 Mpc. As the radial velocity of the NGC 7552 galaxy used by Feinstein (1997) does not differ substantially from the value found by de Vaucouleurs et al. (1991), we did not correct its distance estimate.

5.3 L versus σ diagram

We have mentioned the existence of a correlation between the total luminosity emitted by an H II region in a recombination line and the velocity dispersion of the ionized gas. We have plotted in Fig. 5 the turbulent velocities determined in the present work together with data corresponding to GHIIRs in M33, NGC 6822 and M101 whose luminosities were obtained with narrow-band CCD photometry by Bosch et al. (2002). It can be readily seen that the new GHIIRs lie roughly in the expected area on the L versus σ plane, although it must be kept in mind that the luminosities of Bosch et al. (2002) were determined with a far better knowledge of the distance to the parent galaxy, determined with primary indicators by the *Hubble Space Telescope* Extragalactic Distance Scale Key Project (Freedman, Wilson & Madore 1991; Kelson et al. 1996).

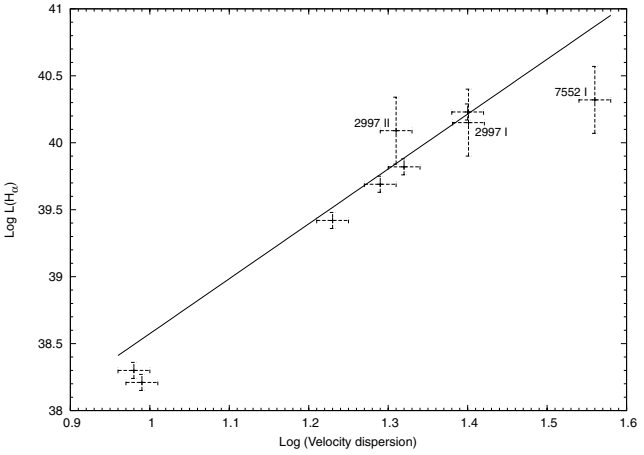

Figure 5. Luminosity versus σ correlations, from the Hα data. Note that the luminosities are not corrected for extinction. We have plotted the turbulent velocities determined in the present work for the three GHIIRs together with data corresponding to GHIIRs in M33, NGC 6822 and M101 whose luminosities were obtained with narrow-band CCD photometry by Bosch et al. (2002).

NGC 7552 IV was not included in the plot, as we consider it not to be a GHIIR. It is worth noting that this region has a high luminosity and would have been considered as a GHIIR if spectroscopic data were not available.

6 SUMMARY

From new high-resolution spectra of the H II regions NGC 2997 I, NGC 2997 II, NGC 7552 I and NGC 7552 IV obtained at the 6.5-m Clay Telescope, LCO, we have confirmed the giant nature of the first three. The MIKE spectrograph has proven to be an excellent tool with which to pursue a search for other GHIIRs in the southern sky. Its usefulness can be improved even more by increasing the wavelength coverage further at the red end, which would allow us to characterize the temperature and densities of the regions using the emission lines lying around 9000 Å.

ACKNOWLEDGMENTS

We are very grateful to C. Feinstein for fruitful discussions and for providing us with the original data and images used for his published work. NM is indebted to the director and staff of LCO for technical assistance and warm hospitality. Special thanks are due to M. Phillips for allowing these science observations during engineering time. We thank an anonymous referee for suggestions that improved this paper noticeably from its original version. This research has made use of the NASA/IPAC Extragalactic Database (NED) which is operated by the Jet Propulsion Laboratory, California Institute of Technology, under contract with the National Aeronautics and Space Administration. IRAF is distributed by NOAO, operated by AURA, Inc., under agreement with the NSF.

REFERENCES

Bosch G., Terlevich E., Terlevich R., 2002, MNRAS, 329, 481
Chu Y. H., Kennicutt R. C. J., 1994, ApJ, 425, 720
de Vaucouleurs G., de Vaucouleurs A., Corwin H. G., Buta R. J., Paturel G., Fouque P., 1991, Third Reference Catalogue of Bright Galaxies, Vol. 1–3, XII. Springer-Verlag, Berlin
Durret F., 1990, A&A, 229, 351
Feinstein C., 1997, ApJS, 112, 29
Freedman W. L., Wilson C. D., Madore B. F., 1991, ApJ, 372, 455
Garnett D. R., 1990, ApJ, 363, 142
Hippelein H. H., 1986, A&A, 160, 374
Kelson D. D. et al., 1996, ApJ, 463, 26
Medina Tanco G. A., Sabalisck N., Jatenco-Pereira V., Opher R., 1997, ApJ, 487, 163
Melnick J., 1979, ApJ, 228, 112
Milliard B., Marcelin M., 1981, A&A, 95, 59
Rola C. S., Terlevich E., Terlevich R., 1997, MNRAS, 289, 419
Roy J. R., Arsenault R., Joncas G., 1986, ApJ, 300, 624
Sandage A., Bedke J., 1988, Atlas of Galaxies Useful for Measuring the Cosmological Distance Scale. NASA, Washington
Smith M. G., Weedman D. W., 1970, ApJ, 160, 65
Sperandio M., Chincarini G., Rampazzo R., de Souza R., 1994, A&AS, 110, 279
Tenorio-Tagle G., Muñoz-Tuñón C., Cox D. P., 1993, ApJ, 418, 767
Terlevich R., Melnick J., 1981, MNRAS, 195, 839

This paper has been typeset from a TEX/LATEX file prepared by the author.